



This discussion paper is/has been under review for the journal Geoscientific Model Development (GMD). Please refer to the corresponding final paper in GMD if available.

Thermo-hydro-mechanical processes in fractured rock formations during glacial advance

A. P. S. Selvadurai¹, A. P. Suvorov¹, and P. A. Selvadurai²

¹Department of Civil Engineering and Applied Mechanics, McGill University, Montréal, QC, H3A 0C3, Canada

²Department of Civil and Environmental Engineering, University of California, Berkeley, CA 94720, USA

Received: 12 October 2014 – Accepted: 15 October 2014 – Published: 5 November 2014

Correspondence to: A. P. S. Selvadurai (patrick.selvadurai@mcgill.ca)

Published by Copernicus Publications on behalf of the European Geosciences Union.

Thermo-hydro-mechanical processes in fractured rock formations

A. P. S. Selvadurai et al.

Title Page

Abstract

Introduction

Conclusions

References

Tables

Figures

⏪

⏩

◀

▶

Back

Close

Full Screen / Esc

Printer-friendly Version

Interactive Discussion



Abstract

The paper examines the coupled thermo-hydro-mechanical (THM) processes that develop in a fractured rock region within a fluid-saturated rock mass due to loads imposed by an advancing glacier. This scenario needs to be examined in order to assess the suitability of potential sites for the location of deep geologic repositories for the storage of high-level nuclear waste. The THM processes are examined using a computational multiphysics approach that takes into account thermo-poroelasticity of the intact geological formation and the presence of a system of sessile but hydraulically interacting fractures (fracture zones). The modeling considers coupled thermo-hydro-mechanical effects in both the intact rock and the fracture zones due to contact normal stresses and fluid pressure at the base of the advancing glacier. Computational modelling provides an assessment of the role of fractures that can modify the pore pressure generation within the entire rock mass.

1 Introduction

The longevity constraints with regard to the safety of deep geologic sequestration of high level radioactive waste suggest that the conventional scientific approaches to the investigations that involve laboratory and field studies must be complemented by approaches that will allow predictions on time scales that are beyond conventional geological engineering activities involving underground facilities (Laughton et al., 1986; Chapman and McKinley, 1987; Rutqvist et al., 2005; Alonso et al., 2005). Current concepts for deep geologic storage require an assessment of the geological setting containing a repository to account for geomorphological processes that can occur over time scales of several thousands of years. The major geomorphological process that is identified over this time scale is glaciation. Our attention is restricted to a geologic setting that has been investigated in connection with the DECOVALEX Project, and the

GMDD

7, 7351–7394, 2014

Thermo-hydro-mechanical processes in fractured rock formations

A. P. S. Selvadurai et al.

Title Page

Abstract

Introduction

Conclusions

References

Tables

Figures

◀

▶

◀

▶

Back

Close

Full Screen / Esc

Printer-friendly Version

Interactive Discussion

domain of interest incorporates a system of fractures that are hydraulically connected but mechanically sessile under the influence of the glaciation loading.

The purpose of this paper is to examine coupled thermo-hydro-mechanical (THM) problems for a fluid-saturated rock mass that contains fracture zones and is subjected to glacial loads. The mechanical response of a fractured rock mass to a glacial cycle was studied in the paper by Steffen et al. (2014); it was shown that fracture zones can lose stability or slip during or after the deglaciation period of the cycle. The glacial cycle scenario was also included in the DECOVALEX studies (Chan et al., 2005) of a fractured rock mass and the current study extends this work to include THM effects and a more accurate treatment of the glacial loading. A secondary objective of the study is to assess the capabilities of a computational multiphysics finite element code COMSOL-Multiphysics in examining a model domain that consists of an intact rock mass and fracture zones, both of which can exhibit THM processes.

The formulation of a coupled hydro-mechanical (HM) problem for fully saturated geological materials was presented by Biot (1941) and reformulated by several investigators including Rice and Cleary (1976) and Hamiel et al. (2005). The HM coupling gives rise to the Mandel–Cryer effect (Selvadurai and Yue, 1994; Selvadurai and Shirazi, 2004), which can explain the momentary increase in the pressure head in an aquifer when the ground water is drained upwards along a fault (Stanislavsky and Garven, 2003) and can predict changes in the fluid pressure induced by the slip of geological faults (Hamiel et al., 2005). Thermo-hydro-mechanical effects have also been of interest to many geoenvironmental processes including the geologic disposal of heat-emitting nuclear waste, frictional heating of faults (Lachenburch, 1980; Rice, 2006), geothermal energy extraction (Dickson and Fanelli, 1995), and ground freezing resulting from buried chilled-gas pipelines (Selvadurai et al., 1999a, b). Solutions to pure fluid flow in heterogeneous formations and coupled thermo-poroelastic problems for fluid saturated geological materials have been obtained by several researchers (Booker and Savvidou, 1985; McTigue, 1986; Selvadurai and Nguyen, 1995, 1997; Nguyen and Selvadurai, 1995; Selvadurai, 1996; Khalili and Selvadurai, 2003; Selvadurai and

Thermo-hydro-mechanical processes in fractured rock formations

A. P. S. Selvadurai et al.

Title Page

Abstract

Introduction

Conclusions

References

Tables

Figures

◀

▶

◀

▶

Back

Close

Full Screen / Esc

Printer-friendly Version

Interactive Discussion



Thermo-hydro-mechanical processes in fractured rock formations

A. P. S. Selvadurai et al.

Title Page

Abstract

Introduction

Conclusions

References

Tables

Figures

◀

▶

◀

▶

Back

Close

Full Screen / Esc

Printer-friendly Version

Interactive Discussion

Selvadurai, 2010; Selvadurai and Suvorov, 2012, 2014). Recent mathematical and computational studies of THM behaviour of fluid-saturated media with both elastic and elasto-plastic skeletal behaviour are given by Selvadurai and Suvorov (2012, 2014) and experimental manifestations of the thermo-poroelastic Mandel–Cryer effect are also given by Najari and Selvadurai (2014).

The behaviour of a rock mass can be influenced by the presence of fractures and faults. Coupled THM behaviour of fractured rocks has been studied by several investigators and extensive references to this work can be found in areas related to geosciences and geomechanics (Noorishad et al., 1984; Selvadurai and Nguyen, 1995; Nguyen et al., 2005; Rutqvist et al., 2002; Guvanasen and Chan, 2000; Chan and Stanchell, 2008; Tsang et al., 2009). Thermo-hydro-mechanical processes in fractured rock formations can be analyzed using two approaches: in the first approach, by modeling discrete fractures and specifying their locations within a host rock, which is modeled as a fracture-free medium, and in the second approach by introducing the influence of fractures implicitly through the derived overall constitutive equations for the fractured medium.

Within a discrete fracture modeling approach, three distinct finite element formulations can be identified: special interface or joint elements (Selvadurai and Nguyen, 1995, 1999; Ng and Small, 1997; Nguyen and Selvadurai, 1998; Guvanasen and Chan, 2000; Steffen et al., 2014), the embedded manifold approach (Guvanasen and Chan, 2000; Juanes et al., 2002; Graf and Therrien, 2008; Erhel et al., 2009), and the conventional or direct approach, in which the fractures are modeled with the finite elements of the same spatial order; e.g., 3-D fractures are modeled with 3-D finite elements (Stanislavsky and Garven, 2003; Chan et al., 2005; Chan and Stanchell, 2005; Sykes et al., 2011). The multiphysics finite element code COMSOL-Multiphysics used in this study has an efficient 3-D mesh generator, well suited for discretizing complex geometries containing distinct narrow regions, such as fractures. Thus, in this paper, the THM problems investigated in connection with glacial loading will be examined using the conventional or direct approach.

Thermo-hydro-mechanical processes in fractured rock formations

A. P. S. Selvadurai et al.

Title Page

Abstract

Introduction

Conclusions

References

Tables

Figures

◀

▶

◀

▶

Back

Close

Full Screen / Esc

Printer-friendly Version

Interactive Discussion

Glacial loads on the surface of a rock mass arise due to the accumulation of snow, ice and water (Aschwanden and Blatter, 2009). The water content within a glacier is generally small (approximately 5 g of water per 1 kg of mixture) and the highest water content is found in the vicinity of the interface with the bedrock. The pattern of fluid flow both within and at the base of a glacier can be a complex THM process. Problems associated with the mechanics of glaciers (Weertman, 1972; Marshall, 2005), the motion of glaciers (Picasso et al., 2004; Gomez et al., 2013; Stucki and Schlunegger, 2013; Ahlkrone et al., 2013; Thoma et al., 2014), their constitutive properties (Picasso et al., 2004; Marshall, 2005; Headley et al., 2012), the contact with the bedrock and the evolution of their shapes (Picasso et al., 2004; Dietrich et al., 2010; Headley et al., 2012; Nielsen et al., 2012; Gomez et al., 2013; Stucki and Schlunegger, 2013; Steffen et al., 2006, 2014) have also been studied. The glacier dynamics on a centennial time scale due to climatic warming was studied by Hambrey et al. (2005), whereas the loss of ice mass due to recent high temperatures in Greenland was estimated by Sasgen et al. (2012). As an approximation of the complex shape of the glacier, the profile of the glacier is often considered to be parabolic (Chan and Stanchell, 2005; Chan et al., 2005; Steffen et al., 2014).

In order to examine the response of a poroelastic rock mass subjected to glacial loads, it is important to adequately take into account the interaction of the glacier with the underlying bedrock. On the temporal scale of interest to the glacial loading of a rock mass containing fracture zones, a simpler representation of the glacier can be adopted. Firstly, mechanical loading due to the weight of the ice sheet needs to be prescribed (Bangtsson and Lund, 2008; Read, 2008). The mechanical loading corresponds to the changing ice-sheet thickness and is applied as a time- and space-varying normal stress at the upper surface of the rock mass (Chan et al., 2005; Chan and Stanchell, 2008; Read, 2008; Person et al., 2012; Steffen et al., 2006, 2014). Secondly, hydraulic boundary conditions must be prescribed. Boulton et al. (1995), Boulton and Caban (1995), Chan et al. (2005) and Person et al. (2012) state that if the permeability of the underlying rock is sufficiently low to discharge all basal melt-water as groundwater

Thermo-hydro-mechanical processes in fractured rock formations

A. P. S. Selvadurai et al.

Title Page

Abstract

Introduction

Conclusions

References

Tables

Figures

◀

▶

◀

▶

Back

Close

Full Screen / Esc

Printer-friendly Version

Interactive Discussion

alone, groundwater heads are approximately equal to the ice pressures and the effective pressures are low. For example, Person et al. (2012) prescribed head boundary conditions on the upper surface of the sedimentary basin assuming that the head is equal to 90 % of the ice sheet elevation.

Chan et al. (2005) also examined the change in the ground surface temperature through the entire glacial cycle using climate/temperature simulation. From this simulation it was clear that before the arrival of the glacier, the ground surface temperature decreases significantly from +10 to -25°C . As the glacier gradually occupies the domain of interest, the insulating effect of the ice sheet gradually increases the subglacial temperature from -25 to 0°C . This complex temperature evolution at the upper surface of the rock mass is simplified in the present work and only a net cool-down from +10 to 0°C , associated with the glaciation period, is considered. Similar surface temperature evolution was used in the study by Read (2008): the mean annual surface temperature was set to $+7^{\circ}\text{C}$ during non-glacial periods and, to account for glaciation, the mean annual rock mass surface temperature was reduced to 0°C .

In this study the rock mass is assumed to be an isotropic thermo-poroelastic domain with a network of dominant fractures that is integral with the surrounding intact rock. The intact rock is assumed to contain only minor fractures, pores and voids, and thus they are not explicitly included into the model. The fracture network is located at the interior of the rock mass domain and remote from its boundaries. Consequently, two distinct regions can be identified in the given rock mass: an interior region with fractures and an exterior region void of fractures. This allows for the observation of the THM response of the fractured region, particularly as the glacier advances, without any dominant influences of the boundaries.

The paper is organized as follows. Mathematical description of thermo-poroelasticity problem is given in Sect. 2 whereas the finite element model is described in detail in Sect. 3. A few numerical tests that validate the model are presented in Sect. 4 and Sect. 5 contains the main computational results that illustrate the influence of glacial loading and temperature change on the development of fluid pressure, velocity,

temperature, displacement and mean effective stress in the entire rock mass and within the individual fractures.

2 Governing equations

2.1 Constitutive models

5 For a linear elastic isotropic fluid-saturated rock, the total stress tensor σ_{ij} is related to the infinitesimal strain tensor ε_{ij} , the fluid pressure p , and the temperature T via the constitutive equation:

$$\sigma_{ij} = 2G_D \varepsilon_{ij} + \left(K_D - \frac{2}{3}G_D \right) \varepsilon_V \delta_{ij} - 3K_D \alpha_s T \delta_{ij} - \alpha p \delta_{ij} \quad (1)$$

10 In Eq. (1), ε_V is the volumetric strain, K_D and G_D denote, respectively, the bulk and shear modulus of the drained rock, α_s is the thermal expansion coefficient of the solid phase of the rock, and α is the Biot coefficient defined as $\alpha = 1 - K_D/K_s$, where K_s is the bulk modulus of the solid phase. The effective stress tensor σ'_{ij} is defined by:

$$15 \quad \sigma'_{ij} = \sigma_{ij} + \alpha p \delta_{ij} \quad (2)$$

and it represents the stress supported by the solid skeleton.

For an isotropic fluid-saturated porous medium, Darcy's law can be written as:

$$v_i = -\frac{k}{\mu} (p_{,i} + \rho_f g \delta_{i3}) \quad (3)$$

20 where v_i is the spatially averaged fluid velocity, k is the permeability of the rock, μ is the dynamic viscosity. Also, ρ_f denotes the fluid density and g is the gravitational acceleration; here it is assumed that the gravitational acceleration vector is pointing in the negative direction of the vertical z axis.

Thermo-hydro-mechanical processes in fractured rock formations

A. P. S. Selvadurai et al.

Title Page

Abstract

Introduction

Conclusions

References

Tables

Figures

◀

▶

◀

▶

Back

Close

Full Screen / Esc

Printer-friendly Version

Interactive Discussion



We assume that the heat transfer in the system is through conduction only and the fluid flow velocity both in the pore space of the intact rock and through the fractures is slow enough so that the convective heat transfer terms can be neglected. It is also assumed that the deformations of the intact rock and the fractures along with the fluid flow processes do not result in the generation of heat. Therefore, heat transfer in the entire rock mass is described by the Fourier law of heat conduction:

$$h_i = -k_c T_{,i} \quad (4)$$

where k_c is the equivalent thermal conductivity of the rock and h_i are the components of the heat flux vector.

Stress equilibrium equations written in terms of displacements u_i are given by

$$\left(K_D + \frac{4}{3}G_D\right) u_{k,ki} + G_D u_{i,kk} - 3K_D \alpha_s T_{,i} - \alpha p_{,i} - \{n\rho_f g + (1-n)\rho_s g\} \delta_{i3} = 0 \quad (5)$$

where n is the porosity, and ρ_s is the density of the solid phase.

From the fluid mass conservation law and Darcy's law (Eq. 3) the fluid flow equation can be derived as

$$\left(\frac{n}{K_f} + \frac{\alpha - n}{K_s}\right) \frac{\partial p}{\partial t} - \frac{k}{\mu} p_{,ii} + \alpha \frac{\partial u_{i,i}}{\partial t} = n3\alpha_f \frac{\partial T}{\partial t} + (\alpha - n)3\alpha_s \frac{\partial T}{\partial t} \quad (6)$$

where α_f is the thermal expansion coefficient of the fluid phase and K_f is the bulk modulus of the fluid phase.

From the thermal energy balance equation and Fourier's law (Eq. 4) the heat conduction equation can be obtained as

$$c_p \frac{\partial T}{\partial t} - k_c T_{,ii} = 0 \quad (7)$$

where c_p is the equivalent specific heat of the rock. Equations (5) to (7) constitute a system of governing equations for a coupled THM problem. If the effect of temperature is neglected, i.e., $T \equiv 0$, we recover the equations applicable to the coupled

Thermo-hydro-mechanical processes in fractured rock formations

A. P. S. Selvadurai et al.

Title Page

Abstract

Introduction

Conclusions

References

Tables

Figures

◀

▶

◀

▶

Back

Close

Full Screen / Esc

Printer-friendly Version

Interactive Discussion

hydro-mechanical (HM) problem. Each of the Eqs. (5)–(7) is valid inside a domain with spatially uniform material properties, i.e., within the fractures or the intact part of the rock. The solution procedures for the coupled THM problem described by the governing Eqs. (5) to (7) are discussed in detail elsewhere (Selvadurai and Suvorov, 2012, 2014) and will not be repeated here.

2.2 The initial boundary value problem

Consider a model of a rock mass in the form of a parallelepiped with upper surface $z = z^{\text{top}}$ and lower surface $z = z^{\text{bot}}$. Assume that a glacier of a non-uniform thickness moves along the upper surface of the rock, $z = z^{\text{top}}$, parallel to the (x, y) plane. The thickness of the glacier is denoted by $H = H(x, y, t)$, where (x, y) are the in-plane coordinates fixed at the base of the rock mass, as indicated in Fig. 1. Since the densities of the glacier constituents, water and ice, are almost equal, the total normal stress acting on the upper surface due to the presence of the glacier is given by

$$\sigma_{zz}(x, y, z^{\text{top}}, t) = -\rho_f g H(x, y, t) \quad (8)$$

Since the intact rock is assumed to have a very low permeability, the fluid pressure acting on the upper surface can be approximated by (Boulton et al., 1995; Boulton and Caban, 1995; Person et al., 2012)

$$p(x, y, z^{\text{top}}, t) = -\sigma_{zz}(x, y, z^{\text{top}}, t) = \rho_f g H(x, y, t) \quad (9)$$

Therefore, the effective stress exerted by the glacier on the upper surface of the rock mass can be evaluated from Eqs. (2) and (9) as

$$\sigma'_{zz}(x, y, z^{\text{top}}, t) = -(1 - \alpha)\rho_f g H(x, y, t) < 0 \quad (10)$$

In addition, the temperature change caused by the presence of the glacier can be prescribed on the upper surface:

$$T(x, y, z^{\text{top}}, t) = T_U(x, y, t) \quad (11)$$

where T_u is a prescribed function. On the lower surface of the rock mass, $z = z^{\text{bot}}$, we prescribe zero values for the vertical displacement u_3 , the fluid velocity and the heat flux:

$$u_3 = 0; \quad \frac{\partial p}{\partial z} = 0; \quad \frac{\partial T}{\partial z} = 0; \quad z = z^{\text{bot}} \quad (12)$$

On the vertical perimeter edges of the rock model we impose zero displacement, fluid velocity, and heat flux in the direction of the normal to the surface:

$$u_n = 0; \quad \frac{\partial p}{\partial n} = 0; \quad \frac{\partial T}{\partial n} = 0 \quad (13)$$

where $\partial/\partial n = \mathbf{n}\nabla$ is the derivative in the direction normal to a surface.

Initial fields within the rock mass correspond to the fields existing at the onset of glacier motion and thus should include stresses due to the weight of the glacier at its initial position, geostatic stresses, hydrostatic fluid pressure, the temperature distribution due to the geothermal heat flux, etc. In this work we focus attention only on the change in the response of the rock mass caused by the small glacier *advance*, and thus zero initial conditions can be prescribed, if the problem is linear.

3 Finite element modeling

3.1 Model geometry

Figure 1 shows geometry of the fractured rock mass model used in the present study. The region of the rock mass is a parallelepiped with in-plane dimensions 22000m \times 22000m and a thickness of 1700m. The fracture network is located at the interior of the rock mass domain, remote from its boundaries. The specific fracture network examined here contains a system of 21 planar fractures within a region of (approximately) 11550m \times 10200m. Details of the fracture network are shown in Figs. 1, 2

Thermo-hydro-mechanical processes in fractured rock formations

A. P. S. Selvadurai et al.

Title Page

Abstract

Introduction

Conclusions

References

Tables

Figures

◀

▶

◀

▶

Back

Close

Full Screen / Esc

Printer-friendly Version

Interactive Discussion

and 8. Each dominant fracture has the shape of a prism or prisma-toid. The thickness of each fracture is set to 10 m. This is a realistic size for a fracture; an example of a 10 m wide fracture zone situated in the Rhone Valley of the Alps, the Simplon normal fault, is given in the paper by Stucki and Schlunegger (2013). The fractures have orientations with dip angles that range from 0 to $\pm 90^\circ$; however, most fractures have a large dip angle, close to $\pm 90^\circ$, i.e., they are sub-vertical. Most sub-vertical fractures span the entire thickness of the rock mass (1700 m). Most fractures that do not span the entire thickness of the rock originate at the upper surface of the rock.

Each fracture zone is defined by its surface which constitutes a planar quadrilateral formed by the four vertices lying in the same plane. To facilitate construction of the fracture surface, a 2-D workplane is constructed for each fracture. Orientation of the workplane is defined by specifying coordinates of the vector normal to the fracture surface. The fracture contour is drawn in the workplane by specifying coordinates of the four vertices of the fracture surface, transformed to the local coordinate system of the workplane. Subsequently, the fracture surface is extruded at a distance equal to the thickness of the fracture zone (10 m), forming a 3-D prism. Then this prism is embedded into a specified place within the geometry of the rock.

If the fracture originates at the upper surface of the rock (as most fractures do), the upper edge of the fracture zone is expected to coincide with the upper surface of the rock, which is horizontal. However, after the extrusion process described above, if the fracture zone is not strictly vertical, the upper edge of the fracture will be inclined with respect to the horizontal surface of the rock. (This may cause problems later during mesh generation since the edge of the fracture lies too close to the surface of the rock.) To correct this geometry, the fractures' surfaces in their respective workplanes can be extended in such a way that, after extrusion and embedding, the fracture intersects the upper surface of the rock and extends beyond it. Then we simply cut off the portion of the fracture zone above the upper surface of the rock, by using, for example, the subtraction operation. Similar corrections can be performed with respect to other edges of fractures that lie too close to the lower surface of the rock or to the perimeter

Thermo-hydro-mechanical processes in fractured rock formations

A. P. S. Selvadurai et al.

Title Page

Abstract

Introduction

Conclusions

References

Tables

Figures

◀

▶

◀

▶

Back

Close

Full Screen / Esc

Printer-friendly Version

Interactive Discussion



we define the “*Custom*” mesh size for which we assign the following values to the parameters: maximum element size 1690 m, minimum element size 172 m, maximum element growth 1.6, resolution of curvature 0.7, resolution of narrow regions 0.5. The resulting mesh has 158 728 tetrahedral elements and is shown in Fig. 2.

If the error message appears during mesh generation, it is recommended that the mesh size parameters be modified; even a small change in a parameter value can sometimes allow COMSOL to successfully construct the mesh. Otherwise, a change in the geometry should be attempted, such as deletion of the last embedded fracture that caused the error or a small translation of this fracture in the x – y plane. We note that even if a certain fracture was removed from the model due to the error messages, another fracture can still be inserted.

3.3 Glacial loading

The primary emphasis of this work is to examine the THM response of the fractured rock mass when it is subjected to advancing glacial loads. In general, advance or retreat of the glacier can be caused by (a) sliding of the glacier along the bedrock and (b) a change in the accumulation and/or ablation rates. In the first case the shape of the glacier does not change, while in the latter case the shape of the glacier, i.e., its length and height, evolves. In the following we consider the glacier advance caused only by sliding, i.e., case (a).

Figure 1 shows the glacier profile at time $t = 0$ and at time $t > 0$, after the glacier has moved a distance of 7500 m parallel to the x axis. The glacier front is assumed to be parallel to the y axis. Initially, at time $t = 0$, the glacier partially covers the rock over the length of 7500 m; its front is located at $x = -3159$ m (Figs. 1 and 3). It should be noted that the total glacier length is much larger than depicted in Fig. 1 but here only the marginal zone of the glacier that falls within the relatively small (compared to glacier length) dimensions of the model domain is shown.

The thickness of the glacier is non-uniform and can be described by the function $H(X, t)$, where X is the distance from the *center* of the glacier (datum point). Let H_{\max}

Thermo-hydro-mechanical processes in fractured rock formations

A. P. S. Selvadurai et al.

Title Page

Abstract

Introduction

Conclusions

References

Tables

Figures

◀

▶

◀

▶

Back

Close

Full Screen / Esc

Printer-friendly Version

Interactive Discussion

be the maximum thickness of the glacier (at the center), and L be the glacier length, i.e., distance from the glacier center to its front. Then the function $H(X)$ at time $t = 0$ satisfies $H(0) = H_{\max}$ and $H(L) = 0$. The specific form of the function $H(X, t)$ is shown in Fig. 3 and described in Appendix A. In this study the maximum glacier thickness is set equal to $H_{\max} = 3200$ m and $H_{\max}^2/L = 7.7$, which gives the length $L = 1329870$ m. The x -coordinate of the model domain, shown in Figs. 1 and 3, and the glacier X -coordinate are related by $x = X - 1333029$ m.

The velocity of the glacier V is assumed to be $4.0306 \times 10^{-8} \text{ m s}^{-1}$, which is approximately $1.271 \text{ m year}^{-1}$. Thus, in 5900 years the ice sheet front will advance by a distance of 7500 m across the model domain (see Fig. 3). In addition to the actual glacier profile, shown with a solid line, Fig. 3 shows an approximation to this profile with a dashed line. This approximation coincides with the actual glacier profile away from the ice sheet front; however, close to the leading edge of the ice sheet it replaces the actual profile with a much smoother function. In actual numerical computations, the use of this approximation is advantageous since it does not have any sharp corners; smoothing the loading profile has an extremely favorable effect on the convergence properties of the computational scheme, especially when using iterative solvers.

As mentioned, the initial or in-situ state is not modeled in the present study, and therefore the loading applied to the surface of the rock mass only corresponds to the difference between the current position of the glacier, at time t , and its initial position at $t = 0$. (This is an admissible simplification of the problem when the problem is linear.) In this case, the maximum glacier loading will always be applied at the initial position of the glacier front; the amount of the glacier loading will decrease away from the initial positioning of the leading edge.

In the following we focus our attention on the response of the rock mass over a short time (e.g., 5900 years), for a small glacier advance, when the glacier front is still close to the fractured region of the rock and the glacier center remains at a distance from the fractured region. Thus, we do not compute the results corresponding to the maximum value of the glacier loads, when the glacier center itself overruns the model domain.

The choice of the time frame can be explained by the highly non-uniform distribution of the glacier load near the front of the glacier; our intention is to study the effect of this non-uniform load. In addition, we believe that the glacial sliding is limited to *small distances* compared to the overall glacier length.

3.4 Finite element solver

The response of the rock mass was obtained by using the transient finite element (FE) solver in COMSOL. The numerical integration in time was implicit by default, which implies that a matrix factorization is required at each time step. Selecting the proper FE solver is of outmost importance because of the size of memory required, computational time limitations and issues related to convergence. In order to solve the hydro-mechanical (HM) problem Eqs. (5) and (6) for the “*Custom*” mesh, a direct solver, such as the SPOOLES solver, requires a very large memory (larger than 30 GB) and a significant amount of time for matrix factorization. Thus, a direct solver cannot be used for the present problem. After testing several iterative solvers available in COMSOL, it was found that the iterative GMRES solver with the geometric multigrid preconditioner was, in fact, the only solver capable of dealing with this problem within a reasonable time frame. On the memory side, GMRES required only slightly more than 6 GB of RAM. Other preconditioners had slower run times due to convergence issues.

3.5 Material properties

The fracture zones have THM properties substantially different from those of the intact rock. In particular, the permeability of the fracture zones is taken to be about six orders of magnitude greater than the permeability of the intact rock, whereas the Young’s modulus is assumed to be approximately 10 times smaller.

The properties of the intact rock and the fractures used in our computational simulations are the following: Young’s modulus E_D is 30 GPa for the intact rock and 3 GPa for the fractures; Poisson ratio ν_D is 0.25; Biot coefficient α is 0.7; permeability k is

Title Page

Abstract

Introduction

Conclusions

References

Tables

Figures

◀

▶

◀

▶

Back

Close

Full Screen / Esc

Printer-friendly Version

Interactive Discussion



Thermo-hydro-mechanical processes in fractured rock formations

A. P. S. Selvadurai et al.

Title Page

Abstract

Introduction

Conclusions

References

Tables

Figures

⏪

⏩

◀

▶

Back

Close

Full Screen / Esc

Printer-friendly Version

Interactive Discussion

$1.55 \times 10^{-19} \text{ m}^2$ for the intact rock and $3 \times 10^{-13} \text{ m}^2$ for the fractures; dynamic viscosity μ is 0.001 Pa s^{-1} ; fluid bulk modulus K_f is 2.2 GPa; thermal expansion coefficient for the solid phase α_s is $8.3 \times 10^{-6} \text{ }^\circ\text{C}^{-1}$ and for the fluid phase α_f is $69 \times 10^{-6} \text{ }^\circ\text{C}^{-1}$; equivalent specific heat c_p is $1\,830\,500 \text{ N (m}^2 \text{ K)}^{-1}$, equivalent conductivity k_c is $3.66 \text{ W (m K)}^{-1}$ both for the intact rock and for the fracture zones. The porosity is assumed to be 0.05 for both the fracture zones and the intact rock.

4 Model validation

In this section we validate our choice of the user-defined “*Custom*” mesh, consisting of 158 728 tetrahedral elements (Fig. 2), and show that this mesh is suitable for solving the given problem of the bedrock response if the glacier speed is as low as 1.27 m year^{-1} . We will refer to this “*Custom*” mesh as “fracture-biased” mesh.

4.1 Mesh validation for homogeneous rock

The first validation procedure involves analysis of the hydro-mechanical (HM) solutions for the homogeneous rock, i.e. the rock in which properties of the fractures are the same as those of the intact part. Here we examine how the presence of the densely-refined regions in the mesh, in close proximity to the “fracture” zones, may affect the solution. To do so, in addition to the “*Custom*” mesh we consider the regular mesh with only 5786 elements that does not account for the presence of “fracture” zones.

Figure 4 shows the distribution of vertical fluid velocity v_z in the homogeneous rock for the two meshes described above. The time is 5900 years, during which time the glacier has moved a distance of 7500 m. The current position of the glacier front corresponds to transitioning from negative to positive velocity values, which is clearly seen in the figure. The magnitude of the negative velocity is considerably larger than the positive velocity. It can be seen that the fluid velocity distributions for the two meshes are quite similar, i.e., the presence of densely-meshed fracture zones does not change

the solution significantly. This is an expected result since the rock is homogeneous. Our numerical tests also showed that the solution for the “*Custom*” fracture-biased mesh deviates significantly from the regular solution once the glacier speed is increased to 12.7 m year^{-1} . This implies that for larger glacier velocity, the finer mesh will be required.

4.2 Mesh validation for hydraulic problem

The second validation procedure employed involves a comparison of the solutions for two meshes: the user-defined “*Custom*” mesh with 158 728 elements and the predefined “*Extra fine*” mesh with 3 321 534 elements. Taking into account that the “*Extra fine*” mesh has a massive number of elements, which would require a considerable amount of memory, we could solve only the hydraulic problem Eq. (6) in which the deformations of the porous skeleton are suppressed, thus reducing the number of unknowns.

Figure 5 shows the distribution of vertical fluid velocity v_z in the intact rock for the two meshes described above. It can be seen that the vertical fluid velocity distributions for the two meshes are very similar. As before, the fluid velocity behind the glacier front is negative and it is positive ahead of it. The fluid velocity in the intact rock between the fractures is significantly reduced as indicated by the dark blue colour of the fracture-free region with changes to green, yellow and even red colours in the region between the fractures.

5 Numerical example

5.1 Solution of HM problem for “*Custom*” mesh

Figures 6 to 10 show the hydro-mechanical response of the fractured rock subjected to glacial loading, described previously, at time 5900 years. The time-dependent fluid pressure and vertical compressive stress induced by the glacial load are applied to

Title Page

Abstract

Introduction

Conclusions

References

Tables

Figures

⏪

⏩

◀

▶

Back

Close

Full Screen / Esc

Printer-friendly Version

Interactive Discussion



Thermo-hydro-mechanical processes in fractured rock formations

A. P. S. Selvadurai et al.

Title Page

Abstract

Introduction

Conclusions

References

Tables

Figures

◀

▶

◀

▶

Back

Close

Full Screen / Esc

Printer-friendly Version

Interactive Discussion

the upper surface of the rock mass as prescribed by Eqs. (8) and (9). The solution is obtained by solving hydro-mechanical problem Eqs. (5) and (6) on the user-defined “Custom” mesh. For more accurate results, the model domain, shown in Figs. 1 and 2, was augmented along the x axis by 2 blocks of length 22 000 m each behind the glacier front, and by 1 block of length 14 000 m ahead of the glacier front. The total length of the augmented domain is therefore 80 000 m, while the size along the y axis remains the same – 22 000 m. Mesh size parameters retain the same values as for the user-defined “Custom” mesh, described above. The new blocks are fracture-free and are discretized using regular, non-biased meshes. The resulting mesh for the extended domain has 167 303 tetrahedral elements, just slightly more than the fracture-biased mesh for the main block of the domain, containing fractures. The increased length of the model domain enables us to take into account the glacier loading more accurately.

Figure 6 shows the typical fluid pressure distribution at the *interior, fractured region* of the rock and *exterior, homogeneous* region at time 5900 years. To capture the response in the fractured region, the fluid pressure was plotted in the cross-section where the y coordinate was equal to 6200 m, which is approximately at the mid-section of the rock mass (see Fig. 1). As is expected, the fluid pressure close to the lower surface is generally smaller than the pressure applied at the upper surface. The maximum fluid pressure occurs close to the initial location of the ice sheet front, i.e., to $x = -3159$ m. Within and around the fractures the fluid pressure is almost uniform through the thickness as the pressure induced at the lower surface is almost equal to the pressure applied at the upper surface. Such a response is caused by the high permeability of the fractures. However, away from the fracture zones, the pressure at the lower surface remains smaller than that at the upper surface, due to the low permeability of the intact rock. This pressure difference creates a vertical pressure gradient $\partial p / \partial z$ and a fluid flow in the downward direction. For the purpose of comparison, Fig. 6 also shows the distribution of fluid pressure in the homogeneous region of the rock in a cross-section parallel to the x axis; the influence of the fractures in altering the fluid pressure distribution in the region due to glacier loading is quite evident. In particular, we can observe

Thermo-hydro-mechanical processes in fractured rock formations

A. P. S. Selvadurai et al.

Title Page

Abstract

Introduction

Conclusions

References

Tables

Figures

◀

▶

◀

▶

Back

Close

Full Screen / Esc

Printer-friendly Version

Interactive Discussion

that the pressure in the intact rock in close proximity to the fractures is larger than the pressure in the fracture-free, or homogeneous region of the rock, for the same value of the x coordinate. This implies that the vertical fluid velocity in the intact rock near the fractures is generally expected to be smaller than that in the homogeneous region of the rock (see also Fig. 7).

Figure 7 shows the vertical fluid velocity v_z in the intact part of the rock with fracture zones at time 5900 years. The vertical velocity distribution in the rock is complex. The fluid velocity can be both positive and negative. A negative fluid velocity implies that fluid flow takes place into the rock (i.e., downwards) and a positive fluid velocity implies that the fluid flows out of the rock (i.e., upwards). It can be seen that, in general, the magnitude of the negative velocity is much larger than the positive velocity, which is consistent with the direction of the melt-water flow. In fact, beneath the glacier most of the fluid flows into the rock with a velocity of $-3 \times 10^{-13} \text{ m s}^{-1}$ and, exterior to the glacial footprint, most of the fluid flows out of the rock with a velocity $2.5 \times 10^{-14} \text{ m s}^{-1}$. Between the fractures the magnitude of the negative fluid velocity in the intact rock is in general smaller compared to that in the homogeneous region of the rock (as the dark blue color in the exterior region of the rock changes to light blue, yellow and even red in the interior region at close proximity to the fractures).

Figure 8 illustrates the vertical fluid velocity v_z within the fractures of the rock at 5900 years. It can be seen that in the fractures oriented sub-vertically (most fractures are sub-vertical) the fluid velocity is much larger than that in the intact part of the rock (compare Fig. 8 with Fig. 7). In fact, the maximum fluid velocity in the fractures can reach a value of $-5.5 \times 10^{-8} \text{ m s}^{-1}$, which is about 50 000 times larger than in the intact rock, but still within the Darcy regime. The greater fluid velocity in the fractures can be explained by the large permeability of the fractures compared to that of the intact rock. We also observe that the fluid can flow both in the negative and positive directions even within a single fracture that is inclined to its strike with respect to the glacier front, i.e., not parallel to the glacier front. For example, the largest sub-vertical fracture in the model is inclined to the strike at an angle of 34.7° with respect to the y axis. At one

Thermo-hydro-mechanical processes in fractured rock formations

A. P. S. Selvadurai et al.

Title Page

Abstract

Introduction

Conclusions

References

Tables

Figures

◀

▶

◀

▶

Back

Close

Full Screen / Esc

Printer-friendly Version

Interactive Discussion



end of this fracture, the vertical fluid velocity is towards the upper surface of the rock and can reach the value of $+5 \times 10^{-8} \text{ m s}^{-1}$, although this fracture is totally covered by the glacier at 5900 years. The fact that some fluid in the fracture can flow towards the upper surface can be explained by the non-uniform distribution of the ice sheet loading along the x axis and the very high permeability of fractures. It should also be noted that in the fractures with a low dip angle (sub-horizontal orientation) the vertical fluid velocity is generally smaller than that in the sub-vertical fractures.

Figure 9 shows the vertical displacement or deflection in the rock mass with fracture zones at time 5900 years. The displacement is negative under the glacier, which is indicative of the mechanical compression of the rock, and positive outside the glacier, which is indicative of the conventional heave associated with glacial loading (Walcott, 1970; Selvadurai, 1979, 2009, 2012; Selvadurai and Nguyen, 1995). The maximum negative displacement (-0.076 m) is near the front of the glacier at its initial position. It can be observed that the displacements in the fractured and homogeneous regions of the rock are virtually the same, i.e., the displacement field is not strongly influenced by the presence of fractures with low deformability properties.

Figure 10 shows the mean effective stress $(\sigma'_{xx} + \sigma'_{yy} + \sigma'_{zz})/3$ in the intact part of the rock with fractures at 5900 years. The mean effective stress is mostly compressive but tensile stresses do occur in the fractured region at the upper surface (dark red patch). The maximum compressive stress occurs near the lower surface of the rock close to the initial location of the ice sheet front. The distinctive feature of the response of the rock with fractures is the existence of tensile stresses near the upper surface between and around the fractures (dark red patch); however, the magnitude of these tensile stresses is smaller than the compressive stress. It can also be observed that in the homogeneous, exterior region of the rock, the stress is entirely compressive. It should be noted that for any failure analysis the HM stress state resulting from glacial loading should be combined with the in-situ geostatic stress states.

5.2 Solution of THM problem for a “Custom” mesh

In Figs. 11 and 12 we illustrate the response of the rock mass with fracture zones subjected to the glacial load described previously and, in addition, to the effects of cooling associated with the advance of the glacier. The time-dependent fluid pressure, the vertical compressive stress and the temperature change are applied to the upper surface of the rock mass as prescribed by Eqs. (8), (9) and (11). As indicated previously, the initial or in-situ state is not taken into account in the present study, and therefore, only the surface loading and temperature that correspond to the difference between the current position of the glacier, at time t , and its initial position are applied to the surface of the rock. The temperature change on the upper surface caused by glacier advance is assumed to have the following form

$$T_u(x, y, t) = T_{\max} \left[\frac{H(x, t)}{H_{\max}} - \frac{H(x, 0)}{H_{\max}} \right] \quad (14)$$

where $H(x, t)$ is the glacier thickness at time t (Appendix A). The maximum temperature change is set equal to $T_{\max} = -10^\circ\text{C}$ and will be reached at the initial location of the ice sheet front when $t = L/V = 1\,047\,000$ years, i.e., when the center of the glacier overruns the model domain.

Figure 11 shows the temperature change generated within the rock 5900 years after initiation of the glacier motion. The temperature change on the upper surface is prescribed according to Eq. (14). The temperature change beneath the glacier reaches the maximum of -0.66°C at the initial location of the ice sheet front, and is zero beyond the glacier margin. (The current maximum of -0.66°C is much smaller than $T_{\max} = -10^\circ\text{C}$ since the center of the glacier is remote from the model domain boundaries at time 5900 years.) The maximum temperature change occurs at the upper surface of the rock, at the initial location of the ice sheet front. We observe that the distribution of the temperature through the thickness of the rock mass under the glacier is non-uniform, which implies that a steady-state was not reached in 5900 years and at the lower surface of the rock the temperature is still above its steady-state value.

Thermo-hydro-mechanical processes in fractured rock formations

A. P. S. Selvadurai et al.

Title Page

Abstract

Introduction

Conclusions

References

Tables

Figures

◀

▶

◀

▶

Back

Close

Full Screen / Esc

Printer-friendly Version

Interactive Discussion



Figure 12 shows mean effective stress in the intact part of the rock with fractures at time 5900 years. The rock mass is subjected to the compressive stress, the fluid pressure induced by the glacial load and the temperature field (Eq. 14) associated with the glacial advance. We note that the compressive mean stress at the lower surface of the rock mass is almost equal to that in the rock subjected only to the mechanical load and fluid pressure (see Fig. 10). The tensile mean stress, however, which occurs in the fractured region in the vicinity of the upper surface, is increased from 0.15 to 0.28 MPa. In contrast to the effective stress, the vertical fluid velocity is not significantly influenced by the cooling: the velocity field in the rock subjected to the compressive stress, the fluid pressure and the temperature field (Eq. 14) is almost the same as that in the rock subjected only to the mechanical load and fluid pressure (as shown in Figs. 7 and 8).

6 Concluding remarks

In the present work, the behavior of a fractured rock mass subjected to advancing glacial loads was analyzed. The glacial load was taken into account by prescribing a spatially and time-dependent compressive stress and fluid pressure on the upper surface of the rock mass. Resulting fluid pressures, vertical fluid velocities, displacements, and mean stress distribution diagrams were obtained through computational simulations that incorporated THM processes. Results were plotted for the specific time of 5900 years during which the glacier advanced across the model domain by a distance of approximately 7500 m.

The computational results show that there is a difference between the fluid pressures at the upper and lower surfaces of the rock mass due to the low permeability of the intact rock. This pressure difference creates a vertical pressure gradient that contributes to the vertical fluid velocity component, which is a major feature of the fluid flow in the present problem. We also observed a difference in the fluid pressure distributions within the fractured region and the surrounding homogeneous region of the rock. In fact, the fluid pressure within the fracture zones and the intact rock in close proximity

to the fractures is larger than that in the homogeneous region, located remotely from the fracture zones. This can be attributed to the large permeability of the fractures.

The distribution of the vertical fluid velocity *within the intact part* of the fractured rock is complex. In general, the direction of the fluid velocity is negative (downward) beneath the glacier and positive (upward) beyond the glacier margin. The magnitude of the downward velocity is larger than the upward velocity, which is consistent with the direction associated with the melt-water flow. As was already noted, between the sub-vertical fractures and near horizontal fractures the vertical fluid velocity in the intact rock is generally smaller than that in the homogeneous region. The vertical fluid velocity *within the fractures* of the rock is about 50 000 times larger than the velocity in the intact rock. The direction of the fluid velocity in the fractures is mainly negative but large velocities in the positive direction can also occur, especially in the sub-vertical fractures that are not parallel to the ice sheet front. The role of the fracture zones and their dominant influence on the fluid flow in the region during a glaciation event is thus confirmed by the present study.

The mean effective stress in the intact part of the rock mass is mostly compressive, but tensile stresses do occur between and around the fractures, at close proximity to the upper surface of the rock. The maximum compressive stress is at the lower surface of the rock at the initial position of the ice sheet front. The glacial loading induces compression of the rock, i.e., negative strain in the direction of the rock thickness. For the situations examined in the paper, this axial compression is relatively uninfluenced by the presence of fracture zones. In addition to the compressive stress and fluid pressure, the given rock mass was subjected to the cooling associated with a glacier advance. Since the present study considers a small glacier advance of only 7500 m, the associated temperature change is also small, only -0.66°C . It was observed that even for this small temperature change, the mean effective tensile stress noticeably increased at the upper surface of the rock between and around the fractures. However, the effect of the cooling on the vertical fluid velocity distribution in the fractured rock was small. These results suggest that the hydro-thermal interaction in the present problem can be

Thermo-hydro-mechanical processes in fractured rock formations

A. P. S. Selvadurai et al.

Title Page

Abstract

Introduction

Conclusions

References

Tables

Figures

◀

▶

◀

▶

Back

Close

Full Screen / Esc

Printer-friendly Version

Interactive Discussion



neglected, but the effect of cooling on the stress distribution in the intact part of the rock (hydro-mechanical interaction) should be given greater consideration.

Computational modeling of fractured rock regions that accounts for THM processes is an essential tool for examining the response of rock masses at time scales relevant to glaciation scenarios. The computational approach allows the examination of the relative importance of components in the THM model and the study of their influence on both the intact rock and the fracture zones at time scales relevant to glaciation scenarios and ultimately to deep geologic disposal concepts. In the modeling considered in this paper both the fracture zones network and the intact rock are assumed to be sessile. The modelling can be extended to include natural hydraulic heterogeneities of the geologic media (Selvadurai and Selvadurai, 2010, 2014) particularly at close proximity to the fracture surfaces, stress-induced alterations of intact permeability (Selvadurai and Głowacki, 2008; Selvadurai et al., 2011; Massart and Selvadurai, 2012, 2014) and alterations to fracture permeabilities during glacial loadings (Nguyen and Selvadurai, 1998; Selvadurai and Yu, 2005; Selvadurai, 2014). These effects can have an important influence on groundwater flow patterns in the domain. The information on the influences of stress states on permeability evolution in fractures is particularly scant and in a detailed analysis relevant to a deep geologic repository setting this aspect needs to be considered. Also implicit in the study is the absence of both radiogenic and geothermal heating effects; the influences of the latter could be important on the time scale of a glaciation event.

Appendix A:

The initial position of the glacier can be described by the function $H(X)$, where H is the thickness of the glacier and X is the distance from the center of the glacier (the datum point). The function $H(X)$ satisfies $H(0) = H_{\max}$ and $H(L) = 0$, where H_{\max} is maximum thickness of the glacier and L is the distance from the center to the glacier front.

Thermo-hydro-mechanical processes in fractured rock formations

A. P. S. Selvadurai et al.

Title Page

Abstract

Introduction

Conclusions

References

Tables

Figures

◀

▶

◀

▶

Back

Close

Full Screen / Esc

Printer-friendly Version

Interactive Discussion



by the formula

$$H(x, t) = 2^{1/8} H_{\max} \left(\frac{-x[\text{m}] - 3159 + Vt}{L} \right)^{1/2}; \quad x - Vt \leq -10759 \text{ m}$$

$$H(x, t) = A_3(x - Vt)^3 + A_2(x - Vt)^2 + A_1(x - Vt) + A_0; \quad -10759 \leq x - Vt \leq -3759 \text{ m}$$

$$H(x, t) = 200F(x, t); \quad x - Vt \geq -3759 \text{ m}$$

$$F(x, t) = \frac{1}{2} + \frac{1}{\pi} \arctan \left(\frac{1}{1200} (-x[\text{m}] - 4159 + Vt) \right) \quad (\text{A3})$$

Here x is the coordinate of the model domain. The function $F(x)$ smoothly changes from 1 to 0 as x increases and it serves to smooth out the sharp corner of Eq. (A2). The coefficients $A_0 - A_3$ in the cubic polynomial are selected to allow continuity with the parabolic function and its first derivative at $x - Vt = -10759$ m and, at the same time, continuity with the function F and its first derivative at $x - Vt = -3759$ m. We note that the approximation Eq. (A3) coincides with the actual parabolic profile Eq. (A2) away from the ice sheet front; however, near the ice sheet front the actual profile is replaced with a much smoother function (Fig. 3).

Code availability

The source files used in the computations performed in connection with this paper can be found at the following links: https://www.dropbox.com/s/83b1gcruk47sib/glacierproblem_mesh158728_noheat.mph?dl=0 https://www.dropbox.com/s/oy7fo28303td1f/glacierproblem_mesh158728_withheat.mph?dl=0.

Acknowledgements. The authors are indebted to the Associate Editor whose constructive suggestions led to improvements in the presentation. The work described in this paper was initiated through the research support provided by the Nuclear Waste Management Organization, Ontario and through a Discovery Research Grant awarded to APSS by the Natural Sciences and Engineering Research Council (NSERC) of Canada. A co-author (P. A. Selvadurai) is

Title Page

Abstract

Introduction

Conclusions

References

Tables

Figures

◀

▶

◀

▶

Back

Close

Full Screen / Esc

Printer-friendly Version

Interactive Discussion



Thermo-hydro-mechanical processes in fractured rock formations

A. P. S. Selvadurai et al.

Title Page

Abstract

Introduction

Conclusions

References

Tables

Figures

◀

▶

◀

▶

Back

Close

Full Screen / Esc

Printer-friendly Version

Interactive Discussion

- Chan, T. and Stanchell, F. W.: Subsurface hydro-mechanical (HM) impacts of glaciation: sensitivity to transient analysis, HM coupling, fracture zone connectivity and model dimensionality, *Int. J. Rock Mech. Min. Sci.*, 42, 828–849, 2005.
- Chan, T. and Stanchell, F. W.: DECOVALEX THMC TASK E – Implications of Glaciation and Coupled Thermo-hydro-mechanical Processes on Shield Flow System Evolution and Performance Assessment, NWMO TR-2008-03, 2008.
- Chan, T., Christiansson, R., Boulton, G. S., Ericsson, L. O., Hartikainen, J., Jensen, M. R., Mas Ivars, D., Stanchell, F. W., Vistrand, P., and Wallroth, T.: DECOVALEX III BMT 3/BENCHPAR WP4: The thermo-hydro-mechanical responses to a glacial cycle and their potential implications for deep geological disposal of nuclear fuel waste in a fractured crystalline rock mass, *Int. J. Rock Mech. Min. Sci.*, 42, 805–827, 2005.
- Chapman, N. A. and McKinley, I. G.: *The Geological Disposal of Nuclear Waste*, John Wiley, New York, 280 pp., 1987.
- Dickson, M. H. and Fanelli, M. (Eds.): *Geothermal Energy*, John Wiley, New York, 1995.
- Dietrich, R., Ivins, E. R., Casassa, G., Lange, H., Wendt, J., and Fritsche, M.: Rapid crustal uplift in Patagonia due to enhanced ice loss, *Earth Planet. Sc. Lett.*, 289, 22–29, 2010.
- Erhel, J., De Dreuzy, J.-R., and Poirriez, B.: Flow simulation in three-dimensional discrete fracture networks, *SIAM J. Sci. Comput.*, 31, 2688–2705, 2009.
- Gomez, N., Pollard, D., and Mitrovica, J. X.: A 3-D coupled ice sheet-sea level model applied to Antarctica through the last 40 ky, *Earth Planet. Sc. Lett.*, 384, 88–99, 2013.
- Graf, T. and Therrien, R.: A method to discretize non-planar fractures for 3D subsurface flow and transport simulations, *Int. J. Numer. Meth. Fl.*, 56, 2069–2090, 2008.
- Guvanasen, V. and Chan, T.: Three-dimensional numerical model for thermo-hydro-mechanical deformation with hysteresis in a fractured rock mass, *Int. J. Rock Mech. Min. Sci.*, 37, 89–106, 2000.
- Hambrey, M. J., Murray, T., Glasser, N. F., Hubbard, A., Hubbard, B., Stuart, G., Hansen, S., and Kohler, J.: Structure and changing dynamics of a polythermal valley glacier on a centennial timescale: Midre Lovénbreen, Svalbard, *J. Geophys. Res.*, 110, F01006, doi:10.1029/2004JF000128, 2005.
- Hamiel, Y., Lyakhovskiy, V., and Agnon, A.: Rock dilation, nonlinear deformation, and pore pressure change under shear, *Earth Planet. Sc. Lett.*, 237, 577–589, 2005.
- Headley, R. M., Roe, G., and Hallet, B.: Glacier longitudinal profiles in regions of active uplift, *Earth Planet. Sc. Lett.*, 317, 354–362, 2012.

Thermo-hydro-mechanical processes in fractured rock formations

A. P. S. Selvadurai et al.

Title Page

Abstract

Introduction

Conclusions

References

Tables

Figures

◀

▶

◀

▶

Back

Close

Full Screen / Esc

Printer-friendly Version

Interactive Discussion



- Selvadurai, A. P. S.: A geophysical application of an elastostatic contact problem, *Math. Mech. Solids.*, 18, 192–203, doi:10.1177/1081286512462304, 2012.
- Selvadurai, A. P. S.: Normal stress-induced permeability hysteresis of a fracture in a granite cylinder, *Geofluids*, online first, doi:10.1111/gfl.12107, 2014.
- 5 Selvadurai, A. P. S. and Głowacki, A.: Evolution of permeability hysteresis of Indiana Limestone during isotropic compression, *Ground Water*, 46, 113–119, 2008.
- Selvadurai, A. P. S. and Nguyen, T. S.: Computational modeling of isothermal consolidation of fractured porous media, *Comput. Geotech.*, 17, 39–73, 1995.
- 10 Selvadurai, A. P. S. and Nguyen, T. S.: Scoping analyses of the coupled thermal-hydrological-mechanical behaviour of the rock mass around a nuclear fuel waste repository, *Eng. Geol.*, 47, 379–400, 1997.
- Selvadurai, A. P. S. and Nguyen, T. S.: Mechanics of fluid transport in a degradable discontinuity, *Eng. Geol.*, 53, 243–249, 1999.
- 15 Selvadurai, A. P. S. and Selvadurai, P. A.: Surface permeability tests: Experiments and modelling for estimating effective permeability, *P. Roy. Soc. Lond. A Math. Phys.*, 466, 2819–2846, 2010.
- Selvadurai, P. A. and Selvadurai, A. P. S.: On the effective permeability of a heterogeneous porous medium: the role of the geometric mean, *Phil. Mag.*, 94, 2318–2338, doi:10.1080/14786435.2014.913111, 2014.
- 20 Selvadurai, A. P. S. and Shirazi, A.: Mandel–Cryer effects in fluid inclusions in damage susceptible poro-elastic media, *Comput. Geotech.*, 37, 285–300, 2004.
- Selvadurai, A. P. S. and Suvorov, A. P.: Boundary heating of poro-elastic and poro-elasto-plastic spheres, *P. Roy. Soc. Lond. A Math. Phys.*, 468, 2779–2806, doi:10.1098/rspa.2012.0035, 2012.
- 25 Selvadurai, A. P. S. and Suvorov, A. P.: Thermo-poromechanics of a fluid-filled cavity in a fluid-saturated porous geomaterial, *P. Roy. Soc. Lond. A Math. Phys.*, 470, 20130634, doi:10.1098/rspa.2013.0634, 2014.
- Selvadurai, A. P. S. and Yu, Q.: Mechanics of a discontinuity in a geomaterial, *Comput. Geotech.*, 32, 92–106, 2005.
- 30 Selvadurai, A. P. S. and Yue, Z. Q.: On the indentation of a poroelastic layer, *Int. J. Numer. Anal. Met. Geomech.*, 18, 161–175, 1994.

Thermo-hydro-mechanical processes in fractured rock formations

A. P. S. Selvadurai et al.

[Title Page](#)

[Abstract](#)

[Introduction](#)

[Conclusions](#)

[References](#)

[Tables](#)

[Figures](#)

[◀](#)

[▶](#)

[◀](#)

[▶](#)

[Back](#)

[Close](#)

[Full Screen / Esc](#)

[Printer-friendly Version](#)

[Interactive Discussion](#)



Selvadurai, A. P. S., Hu, J., and Konuk, I.: Computational modelling of frost heave induced soil-pipeline interaction, I. Modelling of frost heave, *Cold Reg. Sci. Technol.*, 29, 215–228, 1999a.

Selvadurai, A. P. S., Hu, J., and Konuk, I.: Computational modelling of frost heave induced soil-pipeline interaction, II. Modelling of experiments at the Caen Test Facility, *Cold Reg. Sci. Technol.*, 29, 229–257, 1999b.

Selvadurai, A. P. S., Letendre, A., and Hekimi, B.: Axial flow hydraulic pulse testing of an argillaceous limestone, *Environ. Earth Sci.*, 64, 2047–2058, doi:10.1007/s12665-011-1027-7, 2011.

Stanislavsky, E. and Garven, G.: A theoretical model for reverse water-level fluctuations induced by transient permeability in thrust fault zones, *Earth Planet. Sc. Lett.*, 210, 579–586, 2003.

Steffen, H., Kaufmann, G., and Wu, P.: Three-dimensional finite element modeling of the glacial isostatic adjustment in Fennoscandia, *Earth Planet. Sc. Lett.*, 250, 358–375, 2006.

Steffen, R., Wu, P., Steffen, H., and Eaton, D. W.: The effect of earth rheology and ice sheet size on fault slip and magnitude of postglacial earthquakes, *Earth Planet. Sc. Lett.*, 388, 71–80, 2014.

Stucki, M. D. and Schlunegger, F.: Identification of erosional mechanisms during past glaciations based on a bedrock surface model of the central European Alps, *Earth Planet. Sc. Lett.*, 384, 57–70, 2013.

Sykes, J. F., Normani, S. D., and Yin, Y.: Hydrogeologic modelling, Technical Report NWMO DGR-TR-2011-16 R000, Nuclear Waste Management Organization, Toronto, ON, Canada, 2011.

Thoma, M., Grosfeld, K., Barbi, D., Determann, J., Goeller, S., Mayer, C., and Pattyn, F.: RIM-BAY – a multi-approximation 3D ice-dynamics model for comprehensive applications: model description and examples, *Geosci. Model Dev.*, 7, 1–21, doi:10.5194/gmd-7-1-2014, 2014.

Tsang, Y. W., Birkholzer, J. T., and Mukhopadhyay, S.: Modeling of thermally driven hydrological processes in partially saturated fractured rock, *Rev. Geophys.*, 47, 1–30, 2009.

Walcott, R. I.: Flexural rigidity, thickness and viscosity of the lithosphere, *J. Geophys. Res.*, 75, 3941–3954, doi:10.1029/JB075i020p03941, 1970.

Weertman, J.: General theory of water flow at the base of a glacier or ice sheet, *Rev. Geophys. Space Phys.*, 10, 287–333, 1972.

Thermo-hydro-mechanical processes in fractured rock formations

A. P. S. Selvadurai et al.

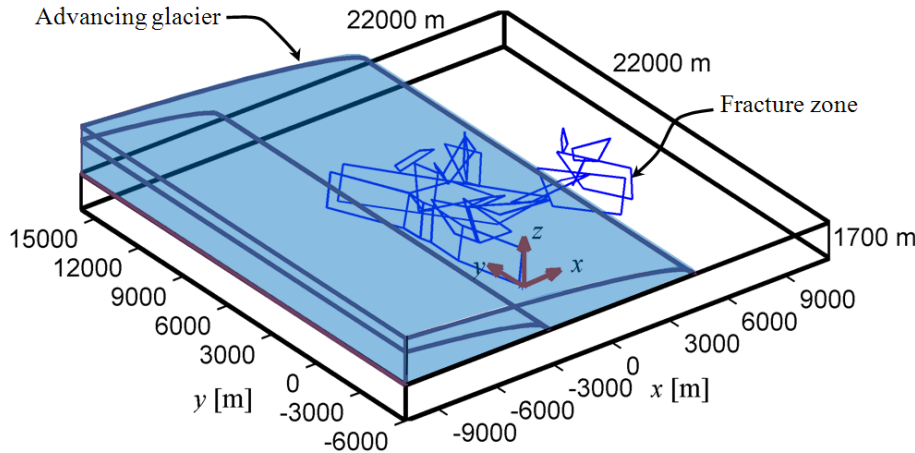


Figure 1. Geometry of the fractured rock mass subjected to loading by the advancing glacier.

Title Page

Abstract

Introduction

Conclusions

References

Tables

Figures



Back

Close

Full Screen / Esc

Printer-friendly Version

Interactive Discussion

Thermo-hydro-mechanical processes in fractured rock formations

A. P. S. Selvadurai et al.

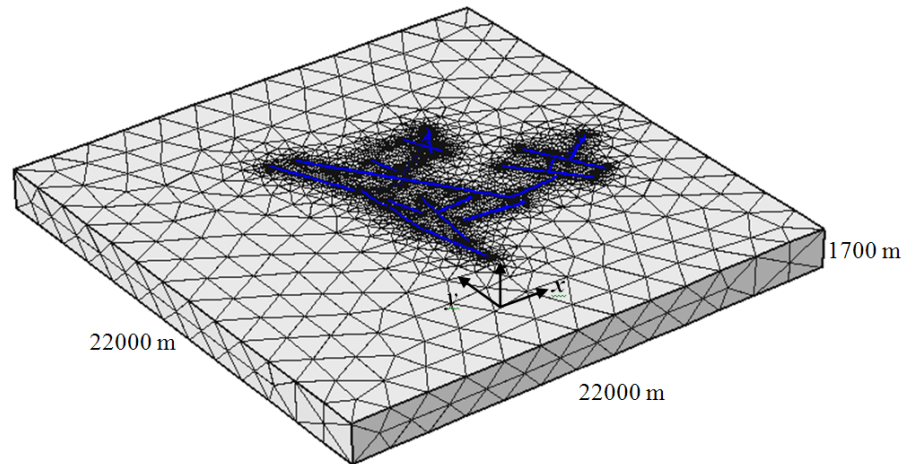


Figure 2. Finite element discretization of the rock mass with a system of interconnecting fracture zones. A discretization of 158 728 tetrahedral elements is used.

[Title Page](#)[Abstract](#)[Introduction](#)[Conclusions](#)[References](#)[Tables](#)[Figures](#)[◀](#)[▶](#)[◀](#)[▶](#)[Back](#)[Close](#)[Full Screen / Esc](#)[Printer-friendly Version](#)[Interactive Discussion](#)

Thermo-hydro-mechanical processes in fractured rock formations

A. P. S. Selvadurai et al.

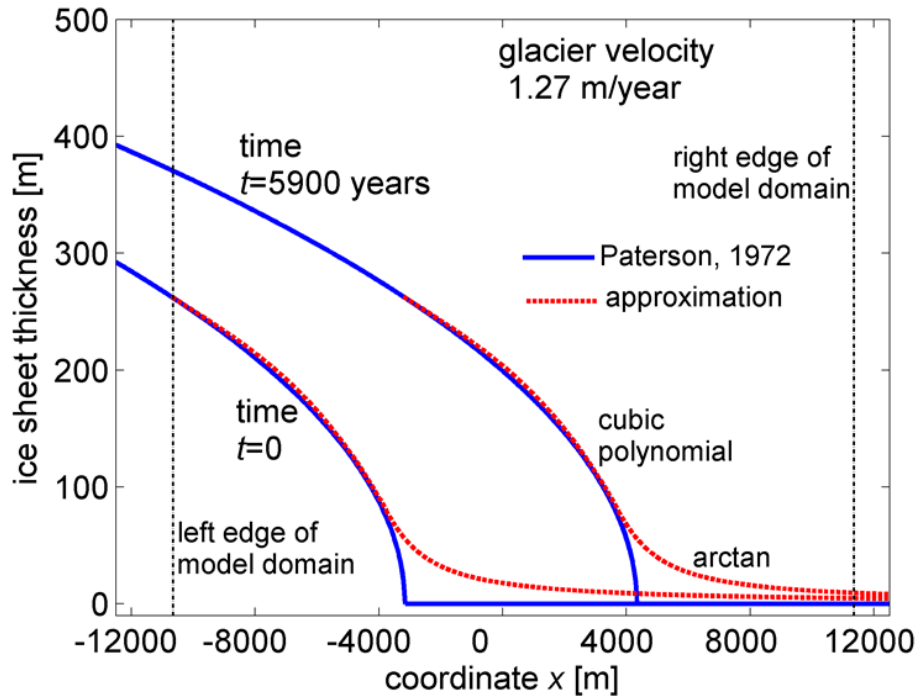


Figure 3. Distribution of the glacier thickness in the ice sheet marginal zone. The exact glacier shape is shown with a solid line, and the approximation to the exact shape, used in the computational simulations, is shown with a dashed line.

Title Page

Abstract

Introduction

Conclusions

References

Tables

Figures

◀

▶

◀

▶

Back

Close

Full Screen / Esc

Printer-friendly Version

Interactive Discussion

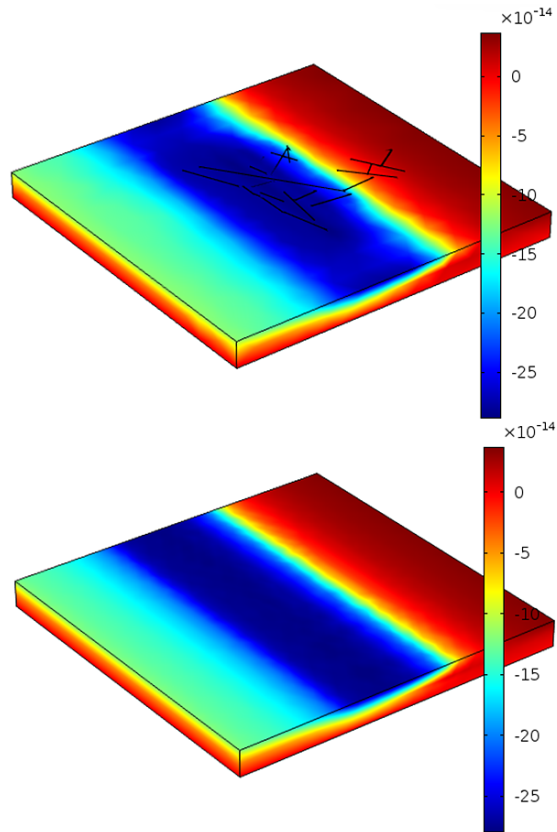


Figure 4. Vertical fluid velocity [m s^{-1}] in the homogeneous rock for the fracture-biased mesh with 158 728 elements (top) and for the regular mesh with 5786 elements (bottom). Time is 5900 years and glacier velocity is 1.27 m year^{-1} .

Thermo-hydro-mechanical processes in fractured rock formations

A. P. S. Selvadurai et al.

Title Page

Abstract

Introduction

Conclusions

References

Tables

Figures

◀

▶

◀

▶

Back

Close

Full Screen / Esc

Printer-friendly Version

Interactive Discussion



Thermo-hydro-mechanical processes in fractured rock formations

A. P. S. Selvadurai et al.

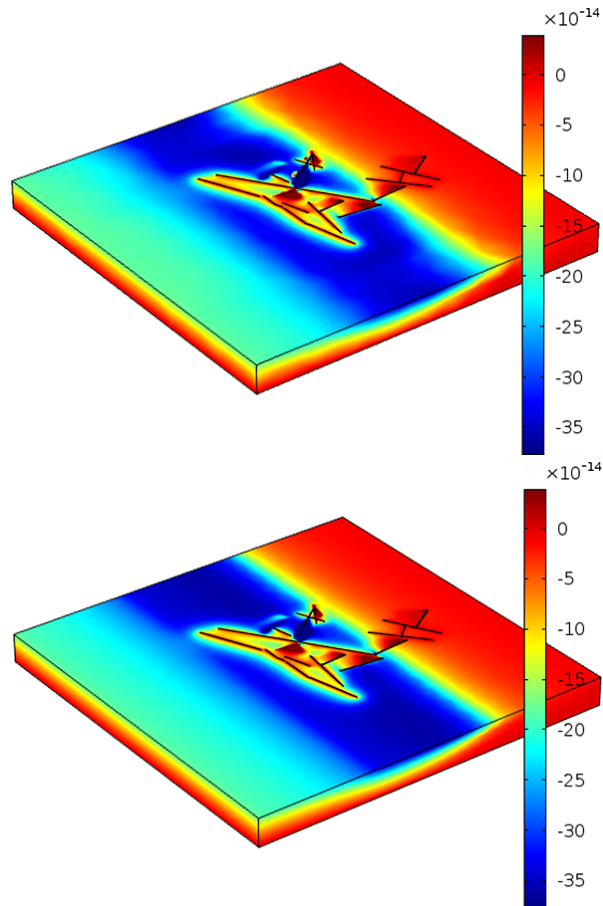


Figure 5. Vertical fluid velocity [m s^{-1}] in the intact part of the fractured rock for “Custom” mesh (top) and “Extra Fine” mesh (bottom). Time is 5900 years and glacier velocity is 1.27 m year^{-1} .

Title Page

Abstract	Introduction
Conclusions	References
Tables	Figures
◀	▶
◀	▶
Back	Close
Full Screen / Esc	
Printer-friendly Version	
Interactive Discussion	



Thermo-hydro-mechanical processes in fractured rock formations

A. P. S. Selvadurai et al.

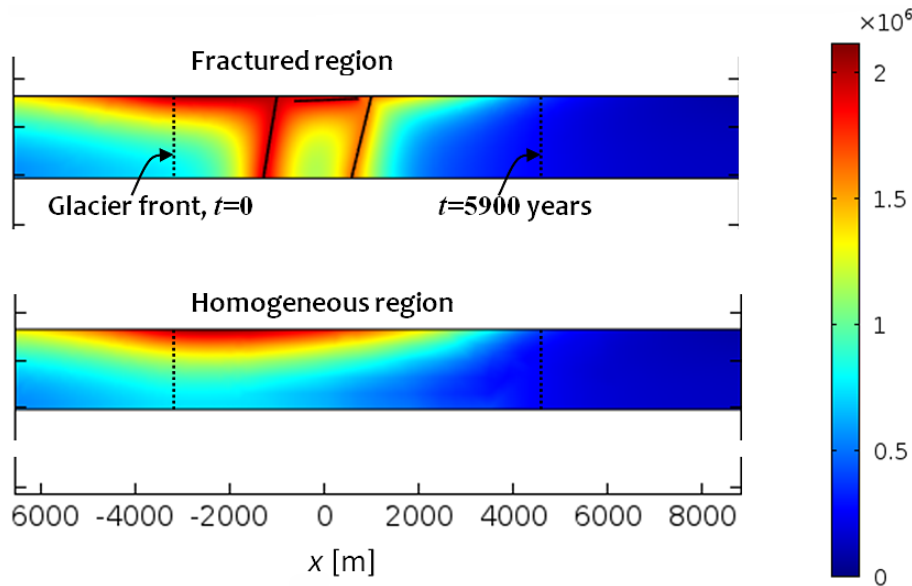


Figure 6. Distribution of fluid pressure [Pa] in the fractured and homogeneous regions of the rock in cross-sections $y = \text{const}$ at time 5900 years. For the fractured region $y = 6200$ m. The rock is subjected to spatially non-uniform fluid pressure and compressive stress.

Title Page

Abstract	Introduction
Conclusions	References
Tables	Figures

⏪
⏩

◀
▶

Back	Close
------	-------

Full Screen / Esc

Printer-friendly Version

Interactive Discussion



Thermo-hydro-mechanical processes in fractured rock formations

A. P. S. Selvadurai et al.

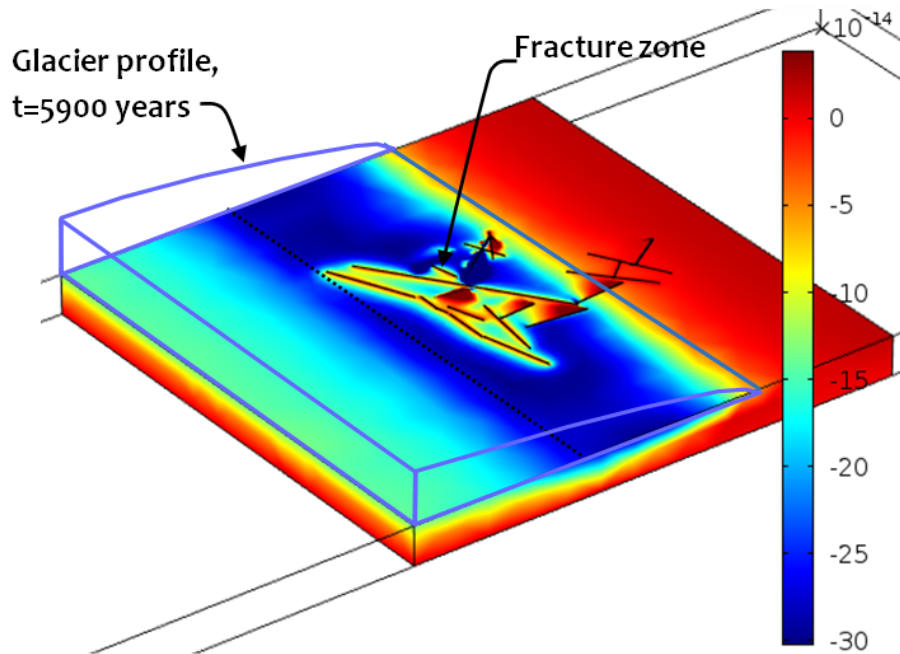


Figure 7. Distribution of the vertical fluid velocity [m s^{-1}] in the rock mass with fracture zones at time 5900 years. The rock mass is subjected to spatially non-uniform fluid pressure and compressive stress imposed by the advancing glacier.

Title Page

Abstract

Introduction

Conclusions

References

Tables

Figures

◀

▶

◀

▶

Back

Close

Full Screen / Esc

Printer-friendly Version

Interactive Discussion

Thermo-hydro-mechanical processes in fractured rock formations

A. P. S. Selvadurai et al.

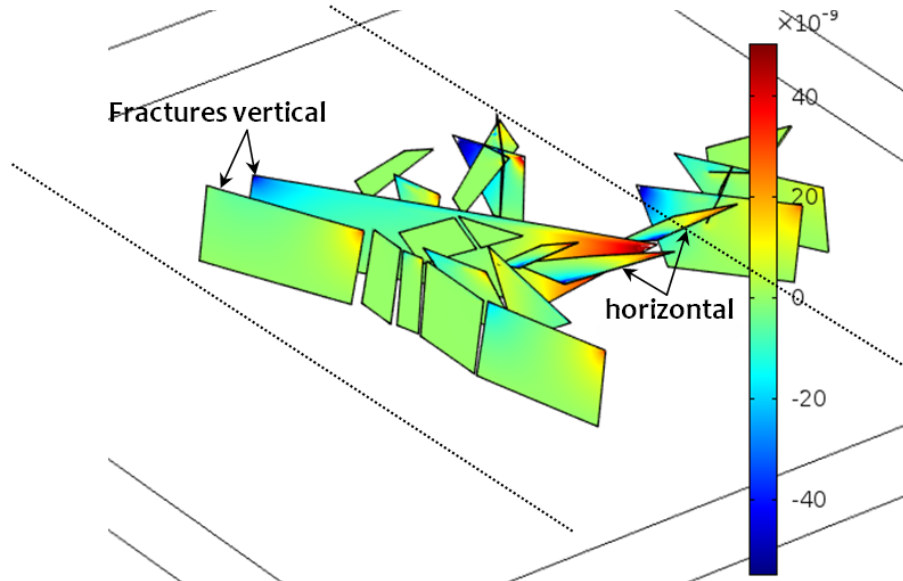


Figure 8. Distribution of the vertical fluid velocity [m s^{-1}] within the fracture zones at time 5900 years. The rock mass is subjected to spatially non-uniform fluid pressure and compressive stress imposed by the advancing glacier.

[Title Page](#)[Abstract](#)[Introduction](#)[Conclusions](#)[References](#)[Tables](#)[Figures](#)[◀](#)[▶](#)[◀](#)[▶](#)[Back](#)[Close](#)[Full Screen / Esc](#)[Printer-friendly Version](#)[Interactive Discussion](#)

Thermo-hydro-mechanical processes in fractured rock formations

A. P. S. Selvadurai et al.

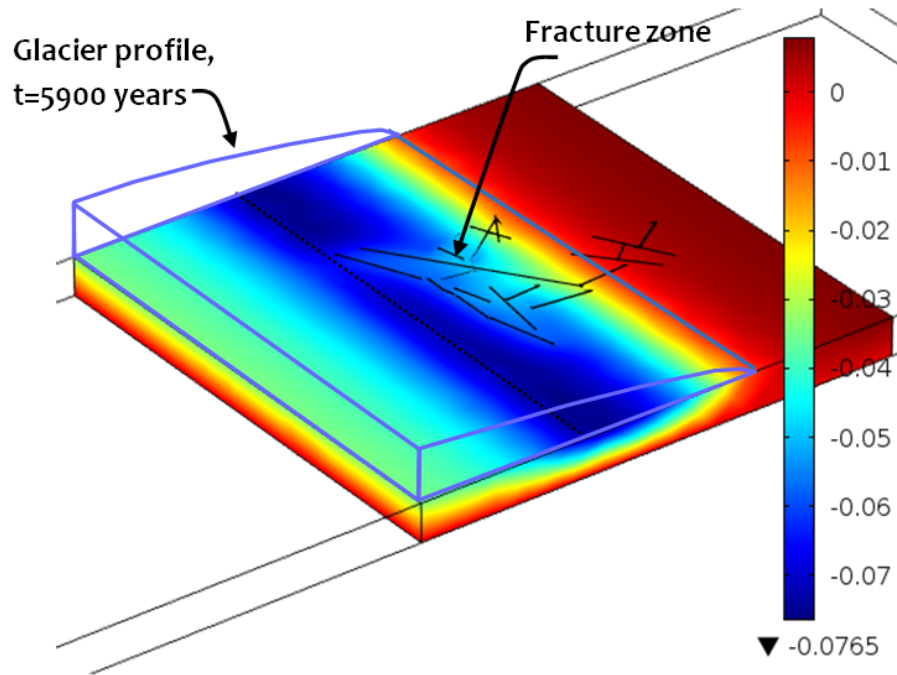


Figure 9. Vertical displacement [m] of the rock mass with fractures at time 5900 years. The rock is subjected to spatially non-uniform fluid pressure and compressive stress.

[Title Page](#)[Abstract](#)[Introduction](#)[Conclusions](#)[References](#)[Tables](#)[Figures](#)[◀](#)[▶](#)[◀](#)[▶](#)[Back](#)[Close](#)[Full Screen / Esc](#)[Printer-friendly Version](#)[Interactive Discussion](#)

Thermo-hydro-mechanical processes in fractured rock formations

A. P. S. Selvadurai et al.

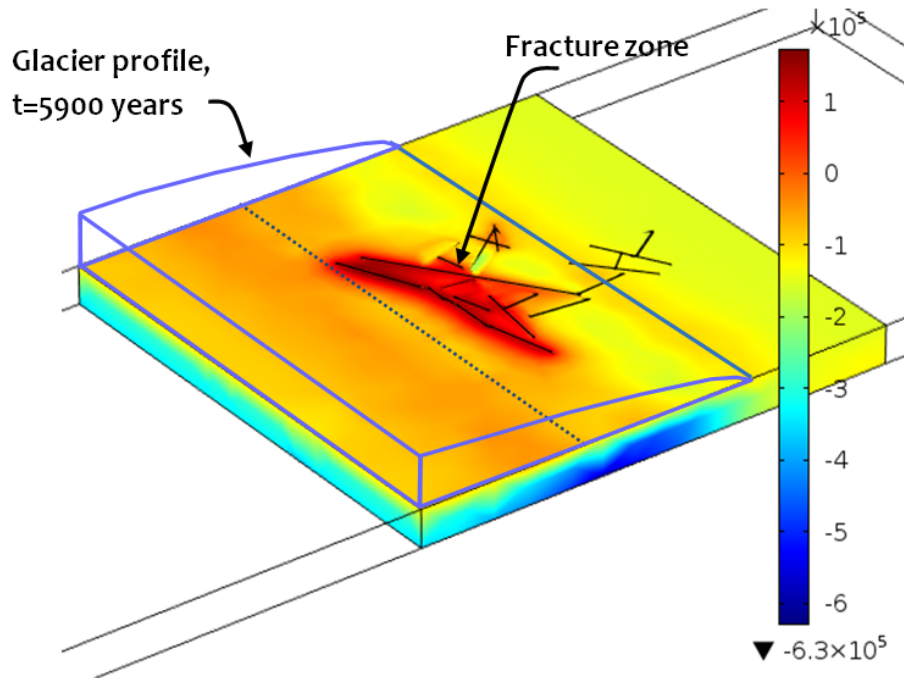


Figure 10. Distribution of the mean effective stress [Pa] within the rock mass with fracture zones at time 5900 years. The rock is subjected to spatially non-uniform fluid pressure and compressive stress.

Title Page

Abstract

Introduction

Conclusions

References

Tables

Figures

◀

▶

◀

▶

Back

Close

Full Screen / Esc

Printer-friendly Version

Interactive Discussion



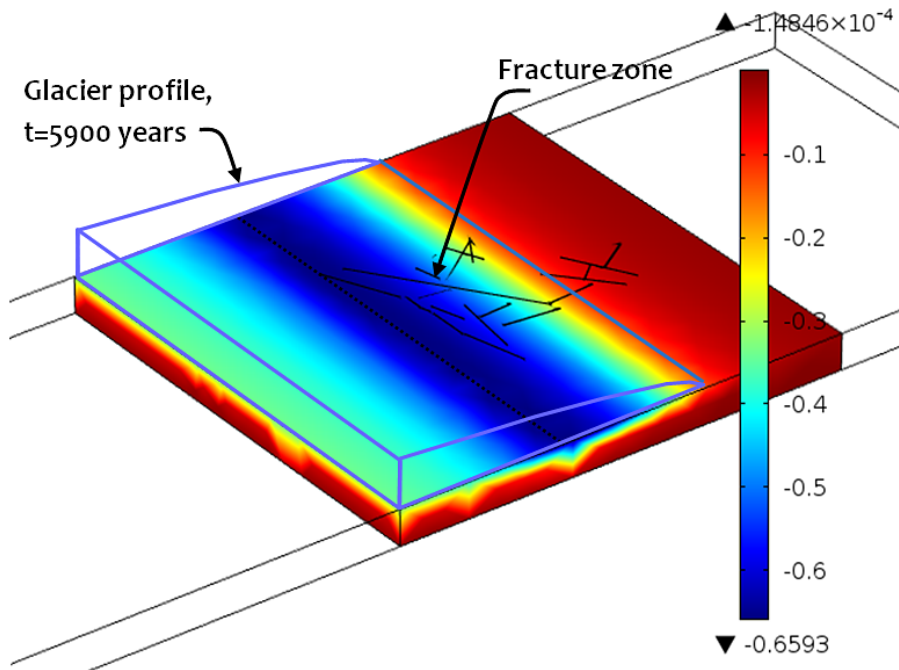


Figure 11. Temperature change distribution [$^{\circ}\text{C}$] within the rock mass 5900 years after the start of the glacier advance.

Thermo-hydro-mechanical processes in fractured rock formations

A. P. S. Selvadurai et al.

Title Page

Abstract

Introduction

Conclusions

References

Tables

Figures

◀

▶

◀

▶

Back

Close

Full Screen / Esc

Printer-friendly Version

Interactive Discussion



Thermo-hydro-mechanical processes in fractured rock formations

A. P. S. Selvadurai et al.

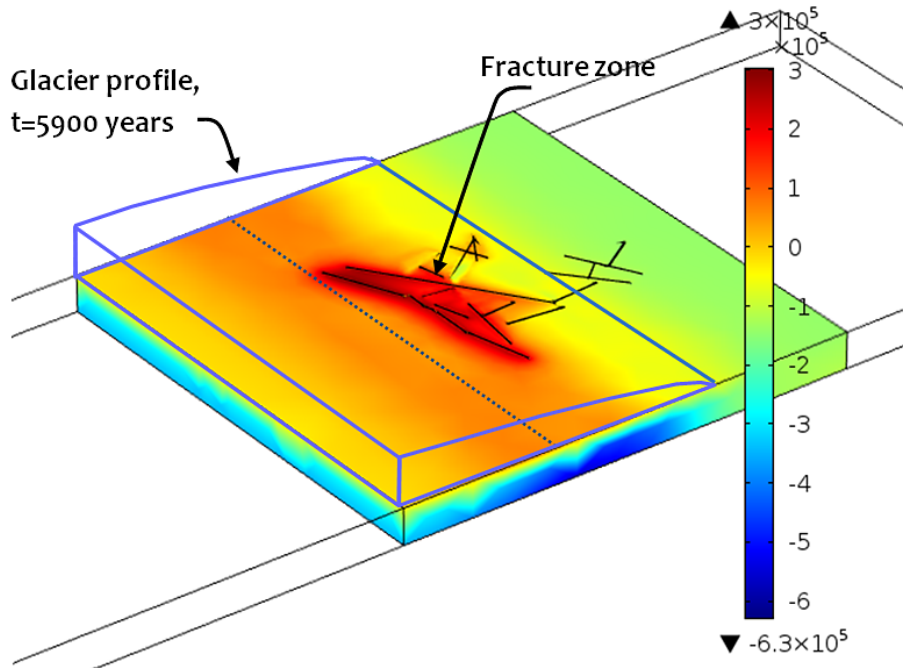


Figure 12. Distribution of the mean effective stress [Pa] within the rock mass with fracture zones at time 5900 years. The rock is subjected to spatially non-uniform fluid pressure, a compressive stress state and a temperature change.

Title Page

Abstract Introduction

Conclusions References

Tables Figures

◀ ▶

◀ ▶

Back Close

Full Screen / Esc

Printer-friendly Version

Interactive Discussion

